ELSEVIER

Journal of Structural Geology 28 (2006) 50–63

JOURNAL OF STRUCTURAL GEOLOGY

www.elsevier.com/locate/jsg

Consistent kinematic architecture in the damage zones of intraplate strike-slip fault systems in North Victoria Land, Antarctica and implications for fault zone evolution

Fabrizio Storti [a,*], Federico Rossetti [a], Andreas L. Läufer [b], Francesco Salvini [a]

[a] *Dipartimento di Scienze Geologiche, Università "Roma Tre", Largo S. L. Murialdo 1, I-00146 Rome, Italy*
[b] *Bundesanstalt für Geowissenschaften und Rohstoffe, Stilleweg 2, 30655 Hannover, Germany*

Received 27 January 2005; received in revised form 8 August 2005; accepted 16 September 2005
Available online 28 October 2005

Abstract

Cumulative, polymodal normal (Gaussian distribution) statistics was applied to subsidiary fault data collected from damage zones associated with the Cenozoic Lanterman and Priestley intraplate right-lateral strike-slip fault systems in North Victoria Land, Antarctica. Results show that five Gaussian peaks out of seven in the Lanterman Fault and five out of nine in the Priestley Fault have almost coincident azimuthal values. We named these Gaussian peak pairs as *consistent fault sets*, arranged in a *consistent kinematic architecture* that is compatible with the Cenozoic regional strike-slip environment. Angular and kinematic relationships among subsidiary fault sets within the consistent kinematic architecture provide constraints for the inference of the state of stress along the Lanterman and Priestley fault systems. We interpret the fault pattern of the consistent kinematic architecture to be produced by early localisation of the principal displacement zone along pre-existing mechanical discontinuities inherited from the Early Paleozoic Ross Orogeny. Shear localisation was followed by subsidiary faulting at an angle to the principal displacement zone according to the Mohr–Coulomb–Byerlee failure criterion.

Keywords: Subsidiary fault; Consistent fault set; Consistent kinematic architecture; Cumulative statistics; Paleostress; Antarctica

1. Introduction

Intraplate strike-slip fault systems can accommodate tens to hundreds of kilometres of horizontal displacement between adjacent lithospheric blocks (Woodcock and Schubert, 1994; Storti et al., 2003a). They typically include almost straight belts alternated with bends and offsets in individual segments, each of them consisting of complex arrays of anastomosing fault strands (Deng et al., 1986; Vauchez et al., 1995; Ludman, 1998; Holdsworth and Pinheiro, 2000; Li et al., 2001; Faulkner et al., 2003). The kinematics of the fault strands depends on their orientation with respect to the total stress field along the principal displacement zone (PDZ in Tchalenko (1970)). The total stress field results from the interplay between the stress field produced by fault motion (i.e. the kinematically-induced stress) and the regional stress field (e.g. Davis, 1984; Mandl, 2000). Strike-slip, transpressional and transtensional fault segments typically coexist along intraplate strike-slip fault systems (Woodcock and Schubert, 1994). This may occur at different scales and may result in the development of very complex fault patterns (in space, time and kinematics; Sylvester, 1988).

In many cases, large-offset faults are not preserved within strike-slip fault systems at the continental scale, due to the progression of the tectonic activity and to preferential erosion and sedimentation in highly fractured fault zones (Price and Carmichael, 1986; Umhoefer, 2000). Nevertheless, small-scale subsidiary faults are widespread in the damage zones of major fault strands (Keller et al., 1995; McGrath and Davison, 1995; Little, 1996; Kim et al., 2004). Detailed fieldwork on the three-dimensional architecture of subsidiary faults along intraplate fault systems provides important information on the modalities of fault propagation and displacement accommodation (Deng and Zhang, 1984; Pachell and Evans, 2002), the role of fault re-activation (e.g.

* Corresponding author.
E-mail address: storti@uniroma3.it (F. Storti).

0191-8141/$ - see front matter © 2005 Elsevier Ltd. All rights reserved.
doi:10.1016/j.jsg.2005.09.004

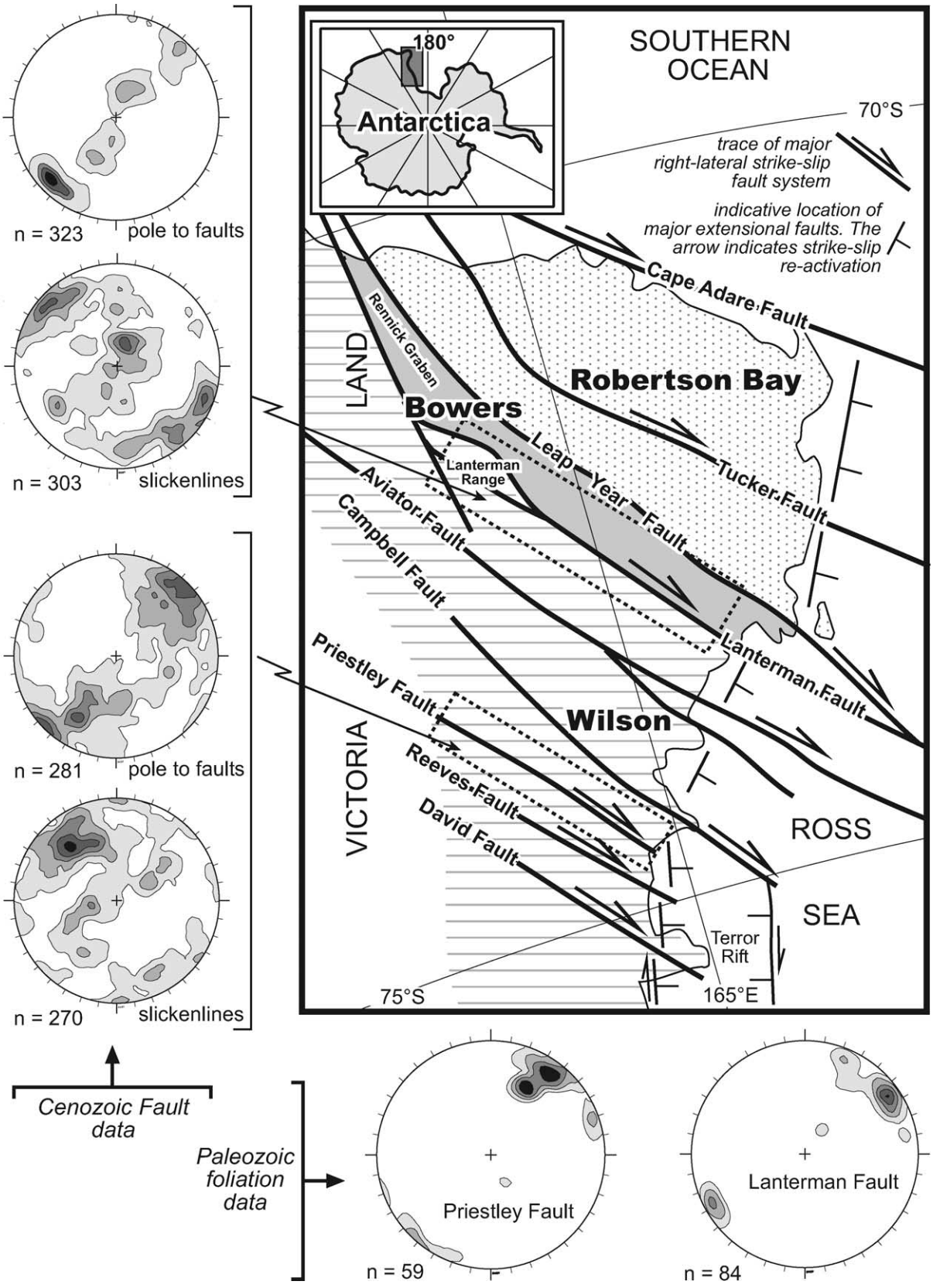

Fig. 1. Tectonic sketch map of North Victoria Land and the western Ross Sea showing the Cenozoic tectonic architecture dominated by NW–SE striking intraplate right-lateral strike-slip fault systems (after Salvini et al., 1997). The two fault system segments analysed in this study are indicated by the broken rectangles. Contours (Schmidt net, lower hemisphere) of poles to faults and slickenlines are provided for each fault segment. Contours (Schmidt net, lower hemisphere) of poles to the main regional foliation occurring in the Early Paleozoic metamorphic rock relicts exposed along the Lanterman and Priestley fault systems are also shown. Contouring interval 4%.

Holdsworth et al., 2001), and on stress conditions along specific fault strands (Rispoli, 1981; Aydin and Schultz, 1990). However, the possible variability of dynamically- and kinematically-induced stress conditions along fault segments and their along- and across-strike geometric irregularity, imply that the generalization of the state of stress obtained at the local scale may lead to biased inferences when extrapolated at the scale of the entire strike-slip fault system. Cumulative statistics of subsidiary fault data in damage zones may provide a useful tool for removing the stress, geometric, and structural variability at the local scale along intraplate strike-slip fault systems, thus contributing to constrain the stress regime under which they developed.

In this paper, we apply cumulative, polymodal normal (Gaussian distribution) statistics to subsidiary fault data collected along the damage zones of the Cenozoic Lanterman (Rossetti et al., 2002) and Priestley (Storti et al., 2001) right-lateral strike-slip fault systems in North Victoria Land, Antarctica (Fig. 1). These continentally sized strike-slip fault systems have similar overall orientations, affect similar rock types, and developed in the same geodynamic scenario. Our results encourage the use of cumulative statistical analysis of large data sets as an additional tool for the complete characterisation of intraplate strike-slip fault systems.

2. Geological framework of the Lanterman and Priestley faults

The tectonic architecture of North Victoria Land has been classically interpreted by the assembly of three major terranes (Fig. 1). These are from west to east the Wilson, Bowers and Robertson Bay terranes (Kleinschmidt and Tessensohn, 1987). The Wilson Terrane generally consists of granitic rocks that are Cambrian to Ordovician in age (Granite Harbour Intrusive Complex; Gunn and Warren, 1962; Rocchi et al., 1998), intercalated with low- to high-grade metamorphic rocks (Gair, 1967; Skinner and Richer, 1968; GANOVEX Team, 1987; Lombardo et al., 1989). The Bowers Terrane generally comprises very low- to low-grade mostly clastic and volcanic Cambrian rocks (Weaver et al., 1984; GANOVEX Team, 1987). Very low- to low-grade Cambrian to Ordovician terrigenous metasedimentary sequences are the dominant rock type exposed in the Robertson Bay Terrane (GANOVEX Team, 1987). The assembly of these terranes occurred during the Early Paleozoic Ross-Delamerian Orogeny (Kleinschmidt and Tessensohn, 1987; Flöttmann et al., 1993). Recent revisiting of the Paleozoic orogenic evolution of Victoria Land questioned the classical terrane model, emphasising a subduction–accretion setting (Finn et al., 1999; Roland et al., 2004).

The Mesozoic break-up of the Antarctic, Australian and Pacific plates resulted in the opening of the Southern Ocean and the Ross Sea, at the northern and eastern boundaries of Victoria Land, respectively (Lawver and Gahagan, 1994; Sutherland, 1995; Mukasa and Dalzier, 2000). In Eocene times (from 50 to 40 Ma), activation of intraplate right-lateral strike-slip tectonics occurred in North Victoria Land and overprinted the still ongoing extension in the Ross Sea (Salvini et al., 1997; Salvini and Storti, 1999; Rossetti et al., 2003). The interplay between right-lateral strike-slip faulting in North Victoria Land and extensional faulting in the Ross Sea resulted in partitioned transtension along the western shoulder of the basin (Wilson, 1995; Salvini et al., 1997; Hamilton et al., 2001; Rossetti et al., 2000, 2003). At this time, emplacement of extrusive and intrusive rocks belonging to the McMurdo Volcanic Group (Kyle and Cole, 1974; Rocchi et al., 2002) also started along the western shoulder of the Ross Sea.

The Lanterman Fault and Priestley Fault are part of the Cenozoic array of NW–SE striking right-lateral strike-slip fault systems that cut through the continental crust of North Victoria Land and continue into the western Ross Sea (Fig. 1) (Salvini et al., 1997). The Lanterman Fault follows the boundary of the Wilson and Bowers terranes and consists of two major segments: a NNW–SSE striking segment in the northern sector and a considerably longer, NW–SE striking segment to the SE (Fig. 1). The fault system records a complex deformation history with both ductile and brittle features preserved (Capponi et al., 1999; Rossetti et al., 2002). Late Cenozoic activity in its offshore segment is indicated by dextral shearing of sediments younger than 32 Ma (Salvini et al., 1997). Apatite thermochronology supports the Late Cenozoic activity of the onshore segments (Rossetti et al., 2003). The onshore length of the Lanterman Fault is approximately 430 km. However, when the offshore segment located in the Ross Sea is included, the total length of this intraplate fault system exceeds 750 km.

The Priestley Fault cuts across the Wilson Terrane, re-activating ductile shear zones that developed during the Ross Orogeny (Storti et al., 2001). Its Cenozoic activity is supported by pseudotachylyte-bearing fault splays exposed at its southern tip, which were dated at ca. 34 Ma (Di Vincenzo et al., 2004). This Cenozoic activity is also supported by the syntectonic injection of McMurdo dykes within the fault zone (Storti et al., 2001). The Priestley Fault has an onshore length of approximately 220 km from the Ross Sea coast to the polar plateau, where the ice cap prevents its further tracing. The Priestley Fault terminates offshore in the Terror Rift transtensional basin, along the western shoulder of the Ross Sea (Storti et al., 2001) (Fig. 1).

Displacement computation is difficult for both fault systems, since the Priestley Fault occurs entirely within granitic rocks, and no significant markers can be correlated across the Lanterman Fault. A cumulative displacement of approximately 270 km has been proposed for the array of Cenozoic right-lateral strike-slip fault systems (Fig. 1) based on restoration of the continental shelf boundary in the Southern Ocean (Storti et al., 2003b).

3. Cumulative data analysis

The study areas include the NW–SE striking segment of the Lanterman Fault and the exposed onshore segment of the Priestley Fault (Fig. 1). Both fault systems crosscut the Cambrian–Ordovician Granite Harbour Intrusive Complex. These rocks are well exposed and are relatively homogeneous in texture. In a few cases, fault data were also collected in scattered metamorphic rock remnants embedded within the granitic bodies. The structural architecture and kinematics of the Lanterman Fault and Priestley Fault are described in Rossetti et al. (2002) and Storti et al. (2001), respectively. For the purposes of this work, the same datasets were statistically analysed.

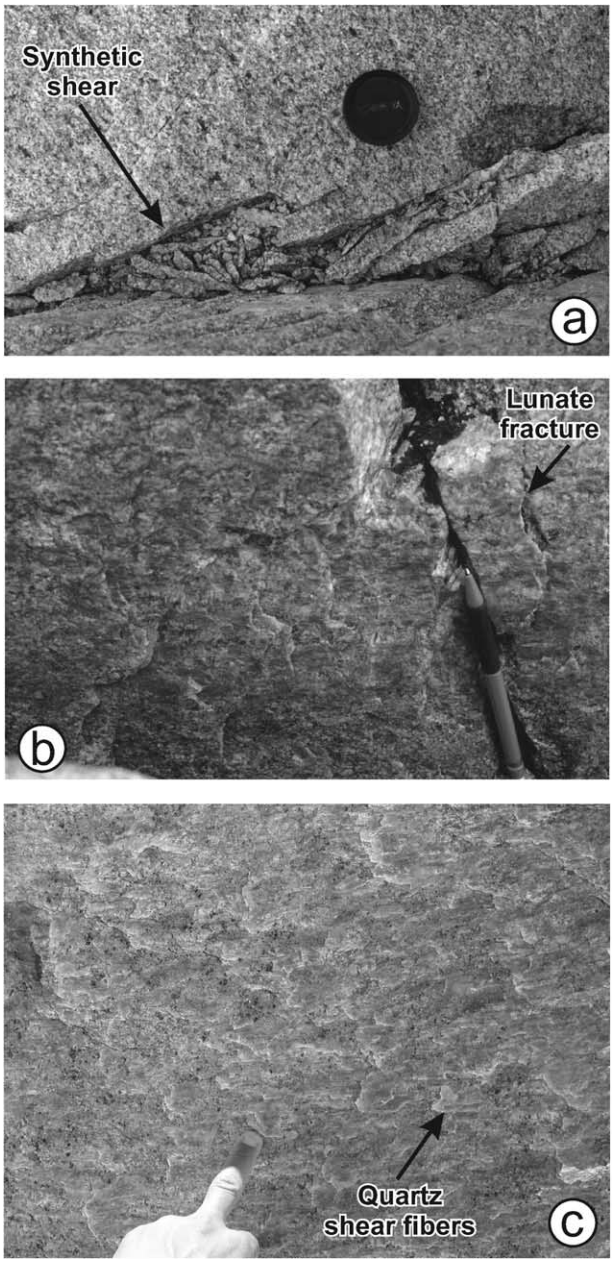

Fig. 2. Kinematic indicators used for shear sense determination of subsidiary faults in granitic rocks. (a) Map view of synthetic shears emanating from the through-going slip surface and forming an acute angle with the fault itself, opening in the same direction as the slip sense of the opposite side (to the right). The resulting slip sense of the fault in this example is left-lateral. (b) Cross-sectional view of a fault surface showing the occurrence of lunate fractures produced by the intersection of the synthetic shears emanating from the through-going slip surface (Petit, 1987). A lunate fracture opens in the same direction as the slip sense of the opposite side (to the left) and the resulting slip sense of the fault in this example is right-lateral. (c) Quartz shear fibres on a fault surface. The growing direction is the same as the slip sense of the opposite side (to the left) and the resulting slip sense of the fault in this example is right-lateral.

Subsidiary faults in the damage zones of both fault systems have an overall NW–SE strike and are predominantly steeply dipping (Fig. 1). This attitude is similar to that of the regional foliation recognized in Early Paleozoic metamorphic rocks exposed along both the Priestley and Lanterman fault systems (Fig. 1). Subsidiary faults mostly include low displacement (some centimetres) single shear surfaces and larger displacement (ten of metres) composite fault zones forming decimetre- to metre-thick cataclastic cores. Kinematic indicators include lunate fractures (Petit, 1987) and quartz slickenfibres (Fig. 2). Slickenlines along the Lanterman Fault are well clustered into major strike-slip and dip-slip populations. Minor oblique-slip populations were also observed. Slickenlines along the Priestley Fault have a similar distribution (Fig. 1).

No systematic overprinting relationship was recognised in the field among the different subsidiary fault sets. The evidence that both the attitude and kinematics of the different subsidiary fault sets are compatible with the regional Cenozoic dextral shearing (Storti et al., 2001; Rossetti et al., 2002), and radiometric (Di Vincenzo et al., 2004) and apatite fission track dating (Rossetti et al., 2003), support the overall contemporaneous activity of the whole fault pattern in post Eocene times (Rossetti et al., 2005).

3.1. Polymodal Gaussian distribution statistics

The normal or Gaussian distribution is by far the most used probability distribution in statistical analysis and is based on the reasonable assumption that the data have a normal distribution around their mean value (Swan and Sandilands, 1995). Applications of Gaussian distribution statistics to structural geology include lineament swarm analysis (Wise et al., 1985) and cleavage population analysis (Salvini et al., 1999; Tavani et al., 2004). In this work we limited Gaussian distribution statistics to fault azimuth data because the PDZ in both the Lanterman and Priestley fault systems is near vertical (Salvini et al., 1997), and because most subsidiary faults in their damage zones have a very steep attitude. The average dip of subsidiary faults in the damage zones of the Lanterman Fault is in fact $77.4 \pm 14.0°$. In the Priestley Fault it is $74.4 \pm 14.7°$, and the mean dip value obtained from merging the two datasets is $77.3 \pm 9.3°$ (Fig. 3a).

In our statistical analysis, all fault data collected along a given fault system were merged into a single dataset from

which data belonging to the four major kinematic types (extensional, reverse, right-lateral strike-slip, and left-lateral strike-slip) were extracted. A frequency analysis showed that right-lateral strike-slip and reverse faults are the dominant kinematic types in both cumulative datasets (i.e. more than 50 fault data in each set) (Fig. 3b). Accordingly, only the strike of right-lateral strike-slip and reverse faults were initially analysed using azimuth-frequency

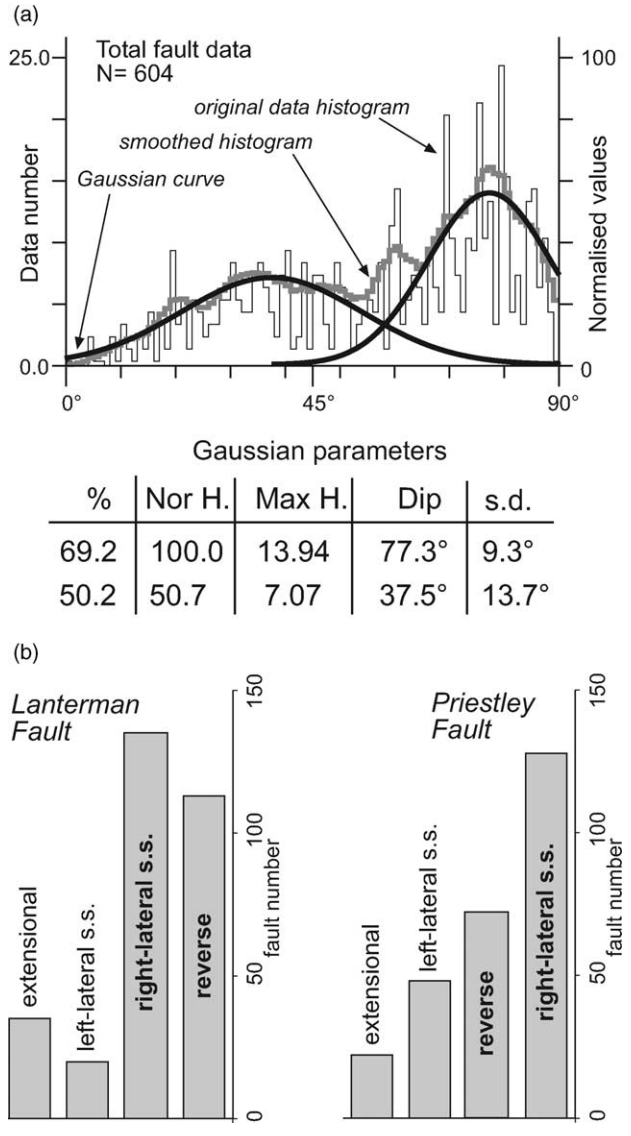

%	Nor H.	Max H.	Dip	s.d.
69.2	100.0	13.94	77.3°	9.3°
50.2	50.7	7.07	37.5°	13.7°

Fig. 3. (a) Cumulative, polymodal Gaussian distribution statistics of fault dip values obtained from the merged datasets of the Lanterman and Priestley right-lateral strike-slip fault systems. The histogram of the original data distribution, the corresponding smoothed histogram, and the Gaussian best-fit curves are shown. In the table, % = percent of data fitted by each Gaussian curve; Nor *H.* = normalised height of the Gaussian peak with respect to the highest peak; Max *H.* = maximum height of the Gaussian peak expressed as smoothed number of data by 10° of interval; s.d. = standard deviation. It is worth noting that the sum of the two % values exceeds 100% because of the overlapping tails of the Gaussian curves. (b) Frequency diagrams of fault kinematic types in the Lanterman Fault and Priestley Fault. In both cases, right-lateral strike-slip and reverse faults are by far more abundant than left-lateral strike-slip and extensional ones.

histograms. Original data histograms were smoothed to reduce noise component of the raw data (Fig. 3a). The smoothing procedure consists of a selected number of moving weighted averages (e.g. Wise et al., 1985). The smoothed value Y_i' at each i interval was computed by (Salvini et al., 1999):

$$Y_i' = \frac{\sum_{j=i-k/2}^{i+k/2} Y_j}{k} \quad (1)$$

where k is the width of the smoothing interval. The smoothed histogram peaks were automatically fitted with Gaussian curves using the approximation of the polymodal probability function in Fraser and Suzuki (1966) and implemented as described in Wise et al. (1985):

$$f(x) = \sum_{i=1}^{N} h_i \exp\left[-4 \ln 2 \left(\frac{x-m_i}{\Delta_i}\right)\right]^2 \quad (2)$$

In this function, x is the variable (fault strike in this study), h is the peak height, m is the mean value of x, N is the number of distributions and Δ_i is the curve width measured at its half height, which relates to the standard deviation of the i Gaussian σ_i according to the following equation (see also Salvini et al., 1999):

$$\Delta_i \cong \sigma_i \sqrt{2_i} \quad (3)$$

In order to reduce the ambiguity between adjacent, independent Gaussian curves and to limit the range of this function within the 0–360° interval, each Gaussian curve was considered only in its $\pm 1.5\ \sigma$ interval (Wise et al., 1985).

Polymodal Gaussian fits were used to identify different fault azimuthal sets within the two analysed kinematic types. The fitting procedure increases the number of Gaussian curves until the residual is below a given threshold value (10%) of the maximum height of the curves. To have a reproducible criterion for selecting the proper number of Gaussian peaks in each analysis, we varied the parameter Δ_i by trial-and-error until the azimuthal difference between adjacent peaks was greater than 15°. This angular difference was derived from the prediction of possible fault types and their expected orientation along a strike-slip fault zone by partitioning the stress field induced by the fault motion into fault-parallel simple shear, fault-parallel compression, and fault-parallel extension (Swanson, 1988) (Fig. 4). Gaussian peaks in the same or different datasets may have very similar azimuthal values thus raising the problem of fault parallelism. We considered Gaussian peaks as azimuthally equivalent when the difference between their azimuthal mean values was lower than the corresponding standard deviations.

3.2. Right-lateral strike-slip faults

Application of the angular limiting criterion described above to the right-lateral strike-slip subsidiary faults of the

Lanterman Fault subset shows that the proper number of Gaussian peaks in this analysis is three (Fig. 5). Lower Δ_i values produce several narrow Gaussian peaks (Fig. 5a and b). Higher Δ_i values cause the loss of significant peaks (Fig. 5d and e). These three Gaussian peaks strike 46.8±9.9°W, 80.5±8.7°W, and 63.7±2.4°W, respectively (Fig. 5c). The same approach gave four Gaussian peaks for the Priestley Fault subset, striking 48.4±9.2°W, 87.5±10.1°W, 24.2±8.6°W and 62.3±2.0°W, respectively (Fig. 6a). The comparison of the azimuthal Gaussian peaks obtained from the two subsets shows remarkable similarities. In particular, three azimuthally equivalent Gaussian peaks can be identified, named *1rl* (NW–SE striking), *2rl* (E–W striking) and *3rl* (WNW–ESE striking), respectively (Fig. 6b). It is worth noting that the angular difference of sets *1rl* and *3rl* in the Lanterman and Priestley fault systems is less than 2° and that the standard deviations of the three Gaussian peaks are also very similar.

3.3. Reverse faults

Polymodal Gaussian distribution statistics of subsidiary reverse faults along the Lanterman Fault revealed four peaks, striking 52.0±10.6°W, 89.7±9.4°E, 70.3±3.7°W and 35.2±2.8°W, respectively (Fig. 7a). The same statistical analysis of the Priestley Fault dataset gave five Gaussian peaks, respectively, striking 53.6±7.7°W, 22.6±5.4°W, 50.0±6.9°E, 19.6±10.3°E, and 88.3±11.3°E (Fig. 7b). The comparison of the azimuthal Gaussian peaks obtained from the two subsets showed the occurrence of two azimuthally equivalent peaks, named *1rev* (NW–SE striking) and *2rev* (E–W striking), respectively (Fig. 7c). The angular difference between Gaussian peaks *1rev* and *2rev* in the Lanterman and Priestley fault systems is less than 2° and their standard deviations are similar (2.9 and 1.9°, respectively).

3.4. Summary

The comparison between the results of cumulative, polymodal Gaussian distribution statistics of the Lanterman and Priestley subsidiary fault datasets indicates the presence of five azimuthally equivalent Gaussian peak pairs, i.e. equivalent Gaussian peaks occurring in both fault systems that are related to the same fault kinematic type (*1rl*, *2rl*, *3rl*, *1rev* and *2rev*; Fig. 8). We named

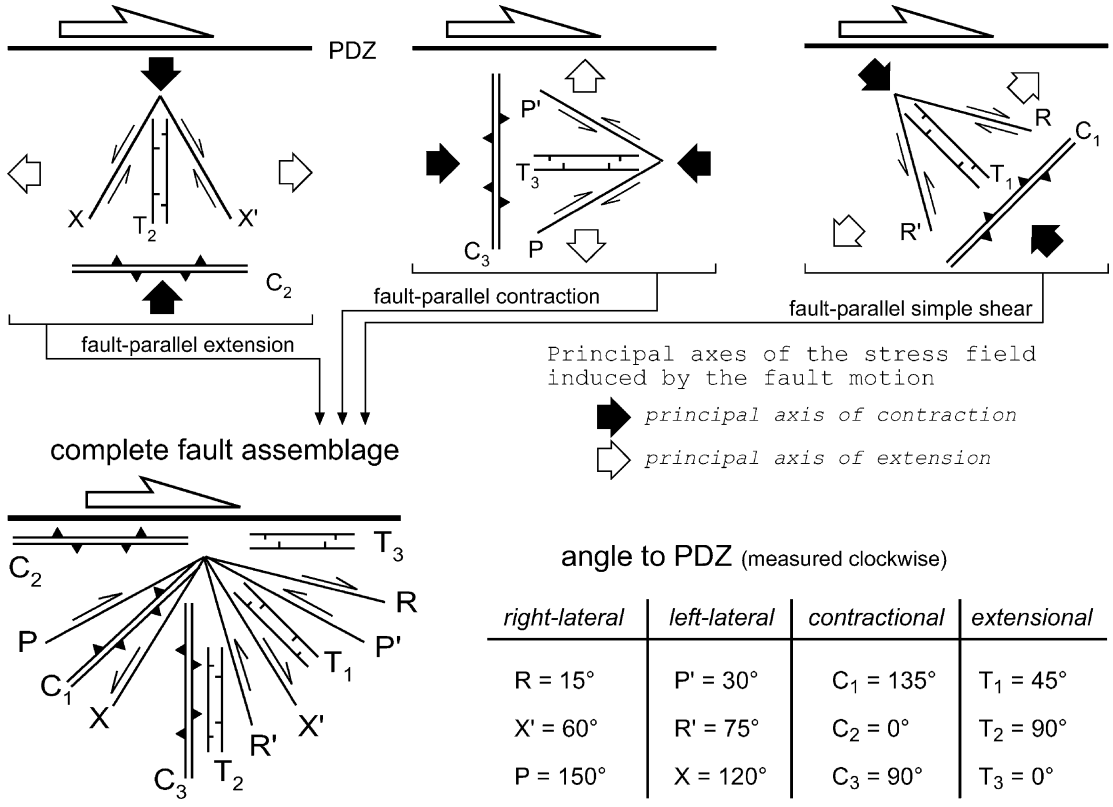

Fig. 4. Cartoon showing possible deformation partitioning into fault-parallel extension, fault-parallel contraction, and fault-parallel simple shear in an idealized dextral fault zone affecting homogeneous material with an angle of internal friction of 30° (after Swanson, 1988). Fault-parallel extension produces the conjugate array of strike-slip faults X (left-lateral) and X′ (right-lateral), bisected by extensional faults/joints T_2, which strike perpendicular to contractional features C_2 (thrusts, folds, cleavage). Fault-parallel contraction produces the conjugate array of strike-slip faults P (right-lateral) and P′ (left-lateral), bisected by extensional faults/joints T_3, which strike perpendicular to contractional features C_3 (thrusts, folds, cleavage). Fault-parallel simple shear produces the conjugate array of strike-slip faults R (right-lateral) and R′ (left-lateral), bisected by extensional faults/joints T_1, which strike perpendicular to contractional features C_1 (thrusts, folds, cleavage).

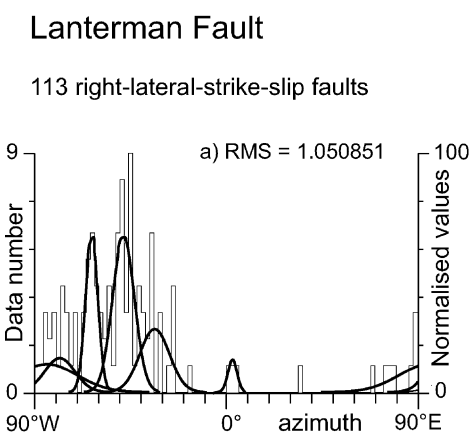

%	Nor H.	Max H.	Azimuth	s.d.
33.2	46.5	5.85	48.3°W	4.27°
18.7	46.3	5.82	63.3°W	2.42°
10.1	10.2	1.28	78.3°W	5.95°
18.3	18.9	2.39	33.7°W	5.79°
16.6	8.3	1.05	84.4°W	11.9°
0.1	8.5	1.07	35.2°E	0.35°
2.8	9.7	1.22	3.0°E	1.76°

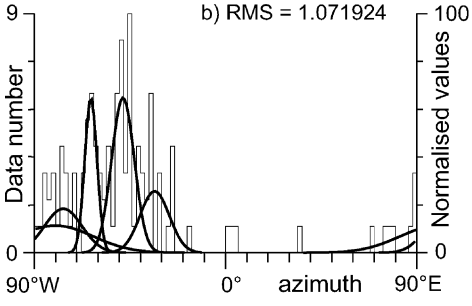

%	Nor H.	Max H.	Azimuth	s.d.
34.2	100.0	5.83	48.3°W	4.41°
18.4	99.8	5.82	63.4°W	2.39°
16.2	28.5	1.66	76.3°W	7.32°
17.6	39.7	2.31	33.3°W	5.73°
20.1	17.5	1.02	80.1°W	14.79°

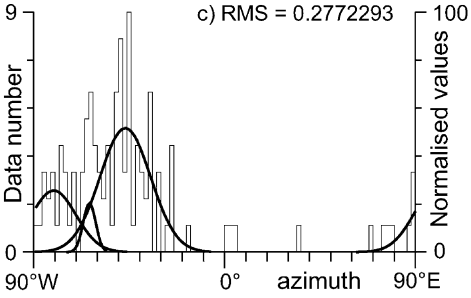

%	Nor H.	Max H.	Azimuth	s.d.
61.5	100.0	4.64	46.8°W	9.94°
26.7	49.6	2.30	80.5°W	8.71°
5.9	39.5	1.83	63.7°W	2.44°

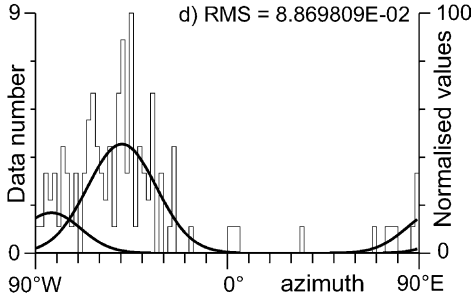

%	Nor H.	Max H.	Azimuth	s.d.
73.1	100.0	4.04	49.4°W	13.44°
23.1	36.9	1.51	82.5°W	11.54°

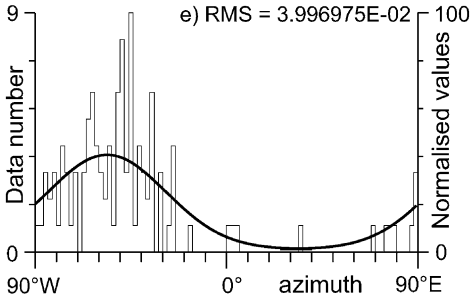

%	Nor H.	Max H.	Azimuth	s.d.
100.0	100.0	3.55	56.2°W	23.13°

Fig. 5. Cumulative polymodal Gaussian distribution statistics of right-lateral strike-slip subsidiary faults collected along the segment of the Lanterman Fault indicated in Fig. 1. (a) Maximum number of identified Gaussian peaks, obtained when Δ_i is very small; (b)–(e) identified Gaussian peaks when Δ_i is progressively increased. Abbreviations in the tables are as in Fig. 3.

these Gaussian peak pairs as *consistent fault sets*. Their strike was obtained by averaging their mean azimuthal values. On the other hand, Gaussian peaks specific to a single dataset are named *inconsistent fault sets*.

The average strike of the consistent fault set *1rl* coincides with that of the trace of both the Lanterman Fault and the Priestley Fault and, consequently, it is considered to indicate the orientation of the PDZ for both fault systems. The angles

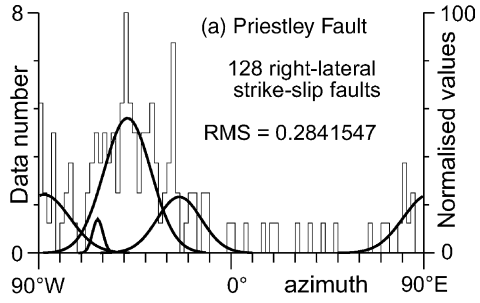

%	Nor H.	Max H.	Azimuth	s.d.
48.4	100.0	4.49	48.4°W	9.18°
22.8	43.2	1.94	87.5°W	10.01°
18.8	41.6	1.87	24.2°W	8.58°
2.6	25.0	1.12	62.3°W	2.0°

(b)

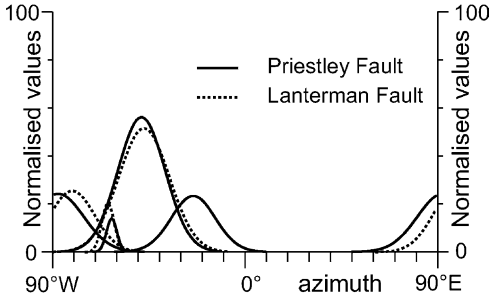

AEP	Priestl.	Lanter.	*differ*	*d_s.d.*
1rl	48.4°W	46.8°W	1.6°	0.76°
2rl	87.5°W	80.5°W	7.0°	1.30°
3rl	62.3°W	63.7°W	1.4°	0.44°

Fig. 6. (a) Cumulative polymodal Gaussian distribution statistics of right-lateral strike-slip subsidiary faults collected along the segment of the Priestley Fault indicated in Fig. 1. Abbreviations in the table of Gaussian parameters are as in Fig. 3. (b) Comparison with results from the Lanterman Fault when the angular difference between adjacent Gaussian peaks is greater than 15° (Fig. 5c). Three azimuthally equivalent Gaussian peaks (AEP) are identified. In the table, *differ* means the difference between the corresponding Gaussian peak pairs in the Lanterman and Priestley data sets, respectively, and *d_s.d.* means the difference between the standard deviations of the corresponding Gaussian peak pairs. See text for further details.

of the other consistent fault sets (measured clockwise) to *1rl* are 174.8° for *1rev* (i.e. azimuthally equivalent to *1rl*), 164.6° for *3rl*, 143.6° for *2rl* and 136.6° for *2rev*, respectively (Fig. 8).

4. Discussion

4.1. Consistent kinematic architecture

The remarkable similarity between the subsidiary fault patterns in the damage zones of the Lanterman and Priestley fault systems may seem somewhat surprising. Although the two right-lateral strike-slip fault systems are more than 200 km apart (Fig. 1), five Gaussian peaks out of seven in the Lanterman Fault and five out of nine in the Priestley Fault cumulative datasets have almost coincident azimuthal values. The fault pattern obtained from cumulative statistics is compatible with that expected for NW–SE striking right-lateral strike-slip shear zones (Sylvester, 1988) (Fig. 9), i.e. the Lanterman and Priestley fault systems. This indicates that such a distribution of fault orientations and kinematics is not a mere statistical artefact. We define this pattern of consistent fault sets as a *consistent kinematic architecture* and interpret it as representative of the state of stress produced by the long-lasting dextral shear affecting the northeastern edge of the Antarctic plate during the Cenozoic (Salvini et al., 1997; Rossetti et al., 2005). Conversely, the attitude and kinematics of inconsistent fault sets are interpreted to be related to local genetic conditions.

Within the consistent kinematic architecture, reverse faults belonging to set *1rev* and paralleling the principal displacement zone are interpreted as related to positive flower structures (Fig. 9) produced by the motion between adjacent fault blocks (Harding, 1985; Sylvester, 1988). Consequently, they are not diagnostic of the sense of shear in the PDZ. The occurrence of positive flower structures parallel to the PDZ was described along both the Lanterman (Rossetti et al., 2002) and the Priestley fault systems (Storti et al., 2001). On the other hand, isolated *1rev* reverse faults, possibly indicative of contraction perpendicular to the PDZ, were not recognised by the same authors. Reverse faults belonging to set *2rev* are interpreted to be produced by the principal compressional axis induced by fault-parallel simple shear during fault motion (e.g. Mandl, 2000) (Fig. 9). Right-lateral strike-slip faults belonging to set *2rl* are interpreted as Andersonian fault sets produced by fault-parallel compression during fault motion (Swanson, 1988; Krantz, 1995) (Figs. 4 and 9). Despite the low statistical validity due to the small number of data, the presence of consistent extensional and left-lateral strike-slip fault sets oriented 46.8°W and 7.1°W, respectively (Fig. 10), provides further support for the occurrence of fault parallel compression. The presence of a NE–SW striking inconsistent set of reverse faults in the Priestley Fault also supports this inference.

Genetic relationships of the fault set *3rl* with the PDZ are not univocal. We interpreted this as a Coulomb-type feature induced by simple shearing during the motion of the fault set *2rl* (Fig. 9). The 7.1°W consistent set of left-lateral strike-slip faults can also be associated with *3rl* to form a conjugate Andersonian array. It is also possible that development of *3rl* was induced by stress increase in the overlapping regions of neighbouring *2rl* faults. The consequent local re-orientation of the principal compressional axis may have caused its closer alignment with the direction of *2rl*, thus having induced synthetic faulting at a smaller angle to the principal displacement zone (Mandl,

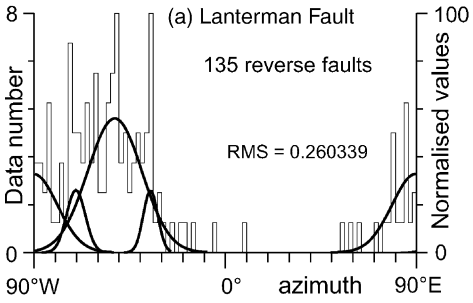

%	Nor H.	Max H.	Azimuth	s.d.
53.0	100.0	4.48	52.0°W	10.61°
27.4	58.7	2.63	89.7°E	9.36°
8.5	46.5	2.08	70.3°W	3.66°
6.5	46.3	2.07	35.2°W	2.82°

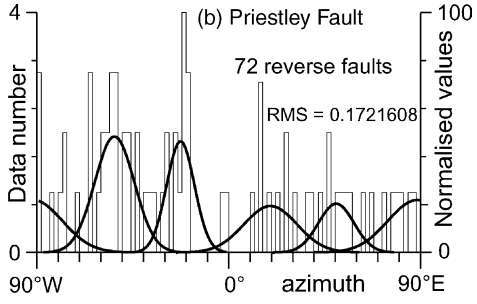

%	Nor H.	Max H.	Azimuth	s.d.
31.2	100.0	1.93	53.6°W	7.73°
21.1	96.0	1.86	22.6°W	5.44°
11.8	42.1	0.81	50.0°E	6.91°
16.7	40.0	0.77	19.6°E	10.34°
20.6	45.2	0.87	88.3°E	11.28°

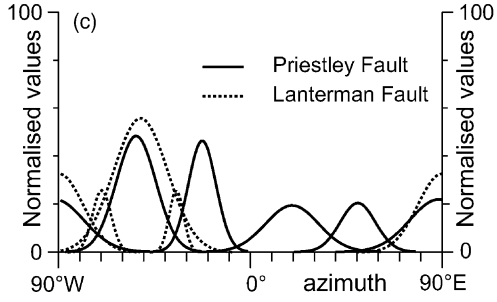

AEP	Priestl.	Lanter.	*differ*	*d_s.d.*
1rev	53.6°W	52.0°W	1.6°	2.88°
2rev	88.3°E	89.7°E	1.4°	1.92°

Fig. 7. Cumulative polymodal Gaussian distribution statistics of reverse subsidiary faults collected along the segments of the Lanterman (a) and Priestley fault systems (b) indicated in Fig. 1. Abbreviations in the tables are as in Fig. 3. Comparison of results indicates the occurrence of two azimuthally equivalent Gaussian peaks (c). Abbreviations in the table are as in Fig. 6. See text for further details.

2000). This interpretation holds for immature fault zone architecture, consisting of overstepping synthetic shears separated by unfractured rock bridges (Mandl, 2000). However, if synthetic faulting is assumed to be triggered by shearing along the PDZ (Martel, 1990), local re-orientation of the principal compressional axis may not be significant within the fault zone due to the mechanical weakness of the PDZ itself. Finally, the fault set *3rl* may have originally developed as *2rl* and then passively rotated to eventually attain its current azimuth. The virtual coincidence of azimuthally equivalent Gaussian peaks in the consistent kinematic architecture of the Lanterman and Priestley fault systems does not support this solution.

4.2. Inferences on paleostress conditions

The orientation of the principal compressional axis σ_1 along the Lanterman and Priestley intraplate right-lateral strike-slip fault systems can be assumed to be mostly dictated by their motion and, consequently, to be perpendicular to the reverse fault set *2rev* (Fig. 9). Accordingly, the strike of σ_1 is predicted to be 1°E, making an angle of 48.6° with the PDZ. Considering the angular difference between the two corresponding mean values of *2rev* in the Lanterman and Priestley fault systems, respectively, (Fig. 7c), the statistic uncertainty in the orientation of σ_1 is $\pm 1.4°$. Verifying the possible occurrence of extensional faults striking parallel to σ_1 can help check this result. Indeed, cumulative statistics of extensional fault data, despite the low data number, indicates the presence of a fault set striking 0.3°W in the Lanterman Fault dataset (Fig. 10a). Using this azimuthal value as indicative of the σ_1 strike provides an angle to the PDZ that differs by 1.3° from the value obtained using the fault set *2rev*. Such an angular difference is lower than the error associated with the result from the consistent kinematic architecture, thus providing further support to the inferred average orientation of σ_1.

4.3. Speculations on fault evolution

The azimuthal values of the fault sets in the consistent kinematic architecture of Fig. 9 are similar to those predicted by the simple shear 'Riedel model' (Logan et al., 1979; Hancock, 1985; Sylvester, 1988). Such a good fit would apparently support the interpretation that the

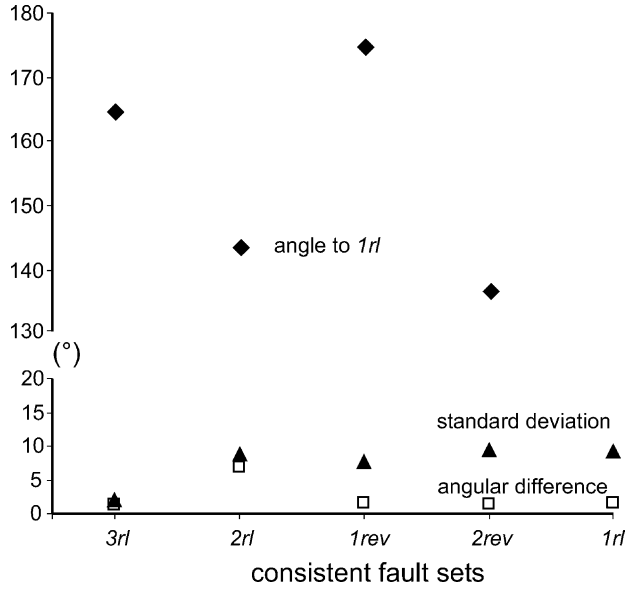

Fig. 8. Main angular parameters of the five azimuthally equivalent Gaussian peaks derived from cumulative polymodal Gaussian distribution statistics of subsidiary fault data along the Lanterman and Priestley fault systems. Angles to *1rl* are measured clockwise. The angular difference between the strike of corresponding peaks is systematically lower than the lower standard deviation value in each Gaussian peak pair.

consistent kinematic architecture was produced by a 'Riedel-type' simple shear framework. Nevertheless, a good match of azimuthal values does not necessarily imply coinciding evolutionary pathways.

Angular and kinematic relationships among fault sets in a typical 'Riedel shear zone' can be explained by the Mohr–Coulomb–Byerlee failure criterion (Tchalenko, 1968; Logan et al., 1979; Sylvester, 1988; Mandl, 2000) by assuming the concomitant contribution of fully partitioned fault-parallel simple shear and fault-parallel compression (Swanson, 1988; Fig. 4). Changing the physical parameters of the faulted rock and/or the boundary stress conditions causes variations of the angular relationships between subsidiary fault sets and the PDZ (Moore et al., 1989; Dresen, 1991; Byerlee, 1992; Moore and Byerlee, 1992; Martel, 1997; Mandl, 2000). Such a dynamic approach does not a priori imply a specific temporal sequence for the development of the different fault sets. The classical sequence of fracturing in a 'Riedel shear zone', from R–R′-shears to P-shears, up to Y-shears, is mainly an outgrowth of analogue experiments (Cloos, 1928; Riedel, 1929; Logan et al., 1979; Naylor et al., 1986; Richard, 1991; Schmocker et al., 2003). A common feature in most analogue experiments of strike-slip faulting is that a pre-existing 'basement fault' induces deformation in the overburden. Thus, a boundary condition in the model set-up results in all structures developed during the experiment to form as secondary features with respect to the geometry of the pre-existing 'basement fault' (An and Sammis, 1996). Changing the experimental boundary conditions to distributed strike-slip shear produces different fault geometries and fracturing sequences (An and Sammis, 1996; An, 1998; Schreurs, 2003).

In the study area, the presence of an inherited NW–SE striking foliation in the basement rocks provided a mechanical anisotropy during Cenozoic strike-slip shearing. This makes a fundamental difference with respect to the 'Riedel-type' boundary conditions. A re-activation scenario, where the PDZ was among the first structures to form (e.g. Martel, 1990; Crider and Peacock, 2004), is more likely for the development of the consistent kinematic architecture. Two pieces of evidence support this inference: (1) the main metamorphic foliation is systematically re-activated by right-lateral strike-slip faults belonging to the consistent right-lateral strike-slip fault set paralleling the PDZ (Storti et al., 2001; Rossetti et al., 2002); (2) the persistence of subsidiary fault sets in the two fault systems (consistent kinematic architecture) rules out the occurrence of significant block rotations about vertical axes along the Lanterman and Priestley fault systems, which would be expected in 'Riedel shear fabrics' with increasing displacement (Freund, 1974; Nur et al., 1986; Swanson, 1988; Arboleya and Engelder, 1995; Peacock et al., 1998; Davis et al., 1999). In the case of the Lanterman and Priestley intraplate strike-slip fault systems, antecedence of the PDZ on the subsidiary fault sets may have occurred at different scales (e.g. compound strike-slip faults of Martel (1990)), eventually producing the entire fault pattern in the damage zones by a hierarchical process (Flodin and Aydin, 2004).

These considerations allow us to infer that the mechanical anisotropy imparted by the principal foliation in the regions where isolated metamorphic rock remnants were preserved, was able to dictate the orientation of the PDZ in both the Lanterman and Priestley strike-slip fault systems. On the other hand, the orientation of the subsidiary fault sets not paralleling the PDZ was mainly influenced by the mechanical properties of the granitic rocks constituting the bulk of the crystalline basement.

5. Conclusions

Results from cumulative, polymodal Gaussian distribution statistics of subsidiary right-lateral strike-slip and reverse fault data collected along the Lanterman and Priestley intraplate right-lateral strike-slip fault systems in North Victoria Land, Antarctica, can be summarised as follows:

(1) Five Gaussian peaks out of seven in the Lanterman Fault and of nine in the Priestley Fault occur in both fault systems and their azimuths differ by less than the corresponding standard deviations. This means that, although the Lanterman and Priestley fault systems are more than 200 km apart, five subsidiary fault sets in the damage zones of both fault systems have very similar to virtually coincident orientations. We name these sets *consistent fault sets*.

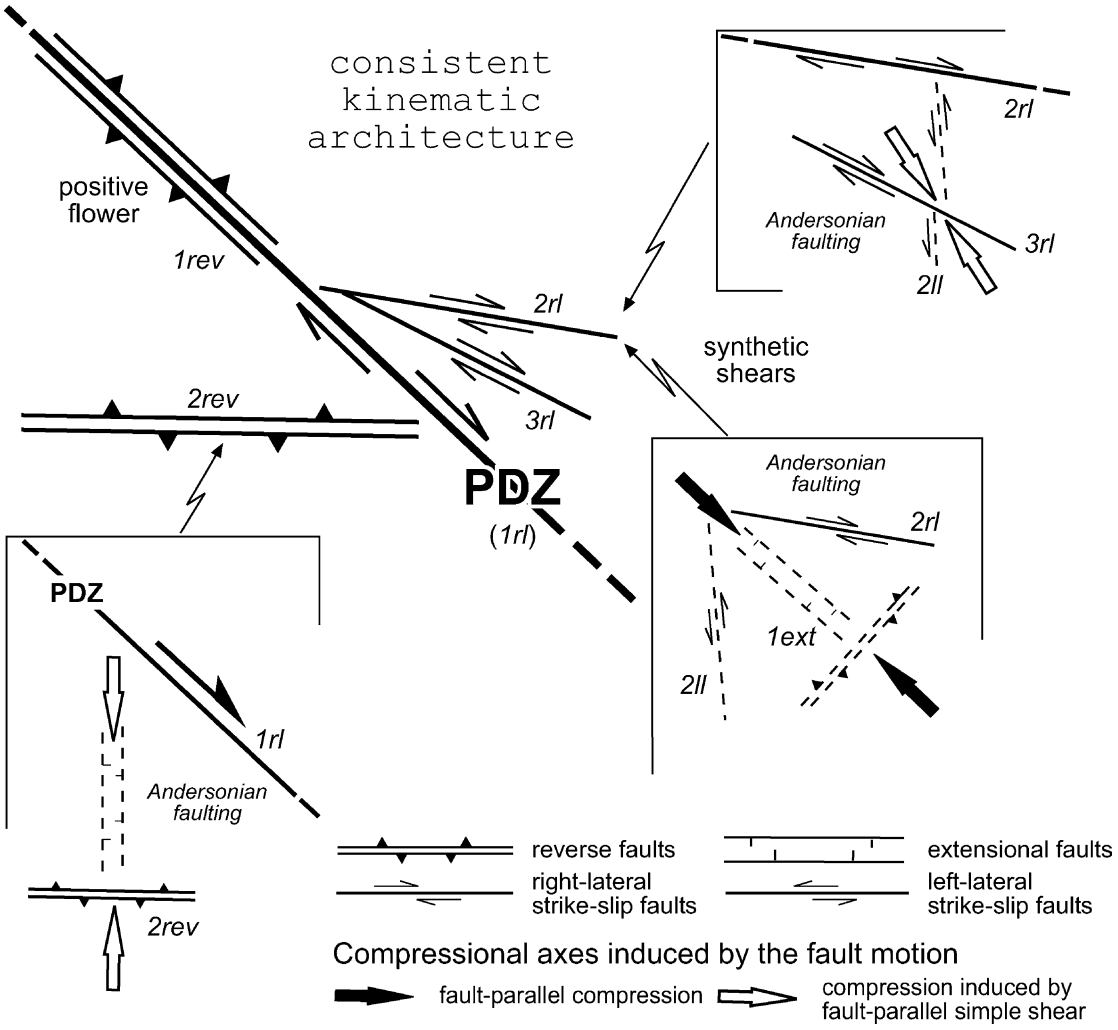

Fig. 9. Consistent kinematic architecture inferred from the strike and kinematics of the consistent fault sets. The proposed genetic mechanisms of the different fault sets are illustrated as well. Broken symbols refer to fault sets obtained from cumulative polymodal Gaussian distribution statistics of extensional and left-lateral strike-slip faults and to an inconsistent set of reverse faults in the Priestley Fault. See text for details.

(2) The orientation and kinematics of the consistent fault sets fit well into the right-lateral strike-slip motion of their parent right-lateral strike-slip fault systems. This means that, despite a basic parameter like the position of subsidiary faults along complex fault systems being neglected in cumulative statistics, the proposed approach produced a geometric and kinematic architecture that properly constrains the overall kinematic and stress fields of such continentally-sized shear zones. This is because the cumulative Gaussian distribution statistics applied to large data sets allowed the removal of the geometric variability of the PDZ, and of possible variations of the state of stress along it.

(3) The assembly of consistent fault sets is named *consistent kinematic architecture* and is interpreted to be mainly dictated by the state of stress in the region undergoing strike-slip tectonics rather than simply deriving from local stress conditions along specific strike-slip fault strands. Accordingly, the consistent kinematic architecture can be used to infer the orientation of the total (regional plus kinematically-induced) stress field in adjacent lithospheric blocks undergoing right-lateral strike-slip shear.

(4) The presence of subsidiary fault sets with virtually identical orientations in the damage zones of both the Lanterman and Priestley fault systems rules out the occurrence of significant block rotations about vertical axes despite the occurrence of several kilometres of displacement along both fault systems. This feature, together with the evidence for re-activation of the pre-existing regional metamorphic foliation, favours an early formation of the PDZ by re-activating pre-existing mechanical discontinuities. The stress field induced by the motion along the PDZ triggered in turn subsidiary faulting at an angle to them, according to the Mohr – Coulomb – Byerlee failure criterion.

%	Nor H.	Max H.	Azimuth	s.d.
60.7	100.0	1.11	0.3°W	12.79°
35.5	60.3	0.67	48.8°W	12.39°

a) Lanterman Fault, 35 extensional faults
RMS = 0.1061453

%	Nor H.	Max H.	Azimuth	s.d.
37.4	100.0	0.43	44.9°W	12.72°
21.6	80.6	0.35	20.0°E	9.13°
12.7	64.0	0.28	69.8°W	6.73°

b) Priestley Fault, 22 extensional faults
RMS = 2.837676E-02

AEP	Priestl.	Lanter.	*differ*	*d_s.d.*
1ext	44.9°W	48.8°W	3.9°	0.33°

c) consistent fault set

%	Nor H.	Max H.	Azimuth	s.d.
41.5	100.0	0.62	42.2°W	8.90°
35.6	69.6	0.43	74.7°E	10.97°
15.3	77.9	0.48	39.6°E	4.22°
4.8	30.4	0.19	4.8°W	3.42°

d) Lanterman Fault, 20 left-lateral strike-slip faults
RMS = 9.963729E-02

%	Nor H.	Max H.	Azimuth	s.d.
21.6	100.0	1.26	47.2°E	5.46°
16.9	44.3	0.56	9.4°W	9.66°
10.5	26.6	0.34	80.3°E	9.96°
9.8	19.1	0.24	62.6°W	13.03°
4.4	22.4	0.28	23.5°E	4.94°

e) Priestley Fault, 48 left-lateral strike-slip faults
RMS = 0.0848317

AEP	Priestl.	Lanter.	*differ*	*d_s.d.*
1ll	80.3°E	74.7°E	5.6°	1.01°
2ll	9.4°W	4.8°W	4.6°	6.24°

f) consistent fault sets

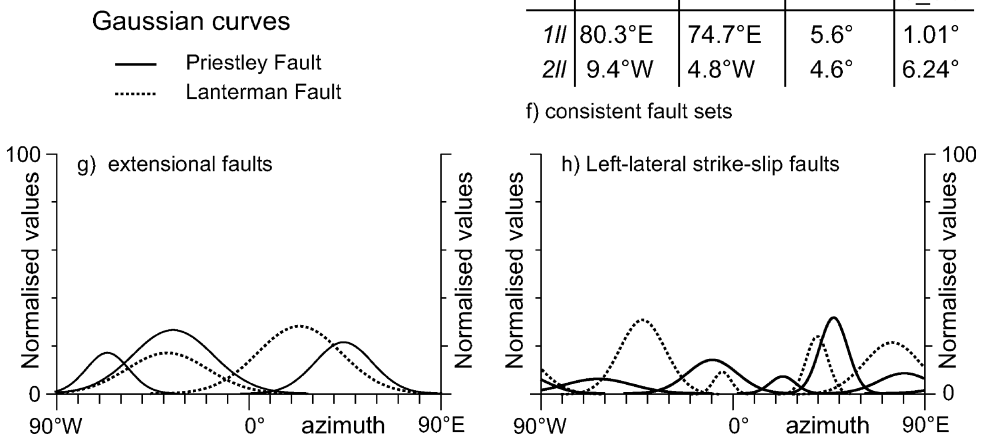

Fig. 10. Cumulative polymodal Gaussian distribution statistics of extensional (a, b) and left-lateral strike-slip (d, e) faults collected along the segments of the Lanterman and Priestley fault systems indicated in Fig. 1. Three azimuthally equivalent Gaussian peaks are identified (c, f, g, h). Their statistical validity is lower than that of consistent fault sets obtained from right-lateral strike-slip and reverse faults due to the much smaller datasets. Abbreviations in the tables are as in Figs. 3 and 6.

Acknowledgements

Constructive criticism and advice from J. Crider, S.J. Martel, T.J. Wilson and N. Woodcock contributed to the final preparation of the manuscript. In particular, the extremely careful review by S.J. Martel helped to improve this paper. Funding for this work was provided by the Italian PNRA and MIUR (awarded to F. Salvini), and by the German Deutsche Forschungsgemeinschaft (grants KL 429/18-1 to 3 awarded to G. Kleinschmidt and A. Läufer). F. Balsamo kindly provided the photo in Fig. 2c. Thanks to S. Boger for going through the English text and giving constructive comments. Parts of this study are based on the joint GANOVEX VIII-ItaliAntartide XV programme (1999/2000). F.R. and A.L. would like to thank the German Bundesanstalt für Geowissenschaften und Rohstoffe (BGR) for invitation to the expedition. A.L. acknowledges provision of polar equipment by Alfred Wegener Institute for Polar and Marine Research. The statistical analyses described in this paper were performed by the DAISY3 software, available for free downloads at http://host.uniroma3.it/progetti/fralab/

References

An, L., 1998. Development of fault discontinuities in shear experiments. Tectonophysics 293, 45–59.

An, L., Sammis, C.G., 1996. Development of strike-slip faults: shear experiments in granular materials and clay using a new technique. Journal of Structural Geology 18, 1061–1077.

Arboleya, M.L., Engelder, T., 1995. Concentrated slip zones with subsidiary shears: their development on three scales in the Cerro Brass fault zone, Appalachian valley and ridge. Journal of Structural Geology 17, 519–532.

Aydin, A., Schultz, R.A., 1990. Effect of mechanical interaction on the development of strike-slip faults with echelon patterns. Journal of Structural Geology 12, 123–129.

Byerlee, J.D., 1992. The change in orientation of subsidiary shears near faults containing pore fluid under high pressure. Tectonophysics 211, 295–303.

Capponi, G., Crispini, L., Meccheri, M., 1999. Structural history and tectonic evolution of the boundary between the Wilson and Bowers terranes, Lanterman Range, northern Victoria Land, Antarctica. Tectonophysics 312, 249–266.

Cloos, H., 1928. Experimente zur inneren Tektonik. Zentralblatt für Mineralogie 12, 609–621.

Crider, J.C., Peacock, D.C.P., 2004. Initiation of brittle faults in the upper crust: a review of field observations. Journal of Structural Geology 26, 691–707.

Davis, G.H., 1984. Structural Geology of Rocks and Regions. Wiley, New York. 492pp.

Davis, G.H., Bump, A.P., Garcia, P.E., Ahlgren, S.G., 1999. Conjugate Riedel deformation band shear zones. Journal of Structural Geology 22, 169–190.

Deng, Q., Zhang, P., 1984. Research on the geometry of shear fracture zones. Journal of Geophysical Research 89, 5699–5710.

Deng, Q., Wu, D., Zhang, P., Chen, S., 1986. Structure and deformational character of strike-slip fault zones. Pure and Applied Geophysics 124, 203–223.

Di Vincenzo, G., Rocchi, S., Rossetti, F., Storti, F., 2004. Dating pseudotachylytes by the ^{40}Ar–^{39}Ar method: the effect of clast–hosted extraneous argon in Cenozoic fault–generated pseudotachylytes from the West Antarctic Rift System. Earth and Planetary Science Letters 223, 349–364.

Dresen, G., 1991. Stress distribution and the orientation of Riedel shears. Tectonophysics 188, 239–247.

Faulkner, D.R., Lewis, A.C., Rutter, E.H., 2003. On the internal structure and mechanics of large strike-slip fault zones: field observations of the Carboneras fault in southeastern Spain. Tectonophysics 367, 235–251.

Finn, C., Moore, D., Damaske, D., Mackey, T., 1999. Aeromagnetic legacy of early Palaeozoic subduction along the Pacific margin of Gondwana. Geology 27, 1087–1090.

Flodin, E.A., Aydin, A., 2004. Evolution of a strike-slip fault network, Valley of Fire State Park, southern Nevada. Geological Society of America Bulletin 116, 42–59.

Flöttman, T., Gibson, G.M., Kleinschmidt, G., 1993. Structural continuity of the Ross and Delamerian orogens of Antarctica and Australia along the margin of the paleo-Pacific. Geology 21, 319–322.

Fraser, R.D.B., Suzuki, E., 1966. Resolution of overlapping absorption bands by least squares procedures. Analytical Chemistry 38, 1770–1773.

Freund, R., 1974. Kinematics of transform and transcurrent faults. Tectonophysics 21, 93–134.

Gair, H.S., 1967. The geology from the upper Rennick Glacier to the coast, northern Victoria Land, Antarctica. New Zealand Journal of Geology and Geophysics 10, 309–344.

GANOVEX Team, 1987. Geological map of North Victoria Land, Antarctica, 1:500,000, explanatory notes. Geologische Jahrbuch B 66, 7–79.

Gunn, B.M., Warren, G., 1962. Geology of Victoria Land between the Mawson and the Mulock Glaciers, Antarctica. New Zealand Geological Survey Bulletin 71, 1–157.

Hamilton, R., Sorlien, C.C., Luyendyk, P., Bartek, L.R., 2001. Cenozoic tectonics of the Cape Roberts rift basin and Transantarctic Mountains front, southwestern Ross Sea, Antarctica. Tectonics 20, 325–342.

Hancock, P.L., 1985. Brittle microtectonics: principles and practices. Journal of Structural Geology 7, 437–457.

Harding, T.P., 1985. Seismic characteristics and identification of negative flower structures, positive flower structures, and positive structural inversion. American Association of Petroleum Geologists Bulletin 69, 582–600.

Holdsworth, R.E., Pinheiro, R.V.L., 2000. The anatomy of shallow crustal transpressional structures: insights from the Archaean Carajas Fault Zone, Amazon, Brazil. Journal of Structural Geology 22, 1105–1123.

Holdsworth, R.E., Stewart, M., Imber, J., Strachan, R.A., 2001. The structure and rheological evolution of continental fault zones: a review and case study. In: Miller, J.A., Holdsworth, R.E., Buick, I.S., Hand, M. (Eds.), Continental Reactivation and Reworking Geological Society, London, Special Publication 184, pp. 115–137.

Keller, J.V.A., Hall, S.H., Dart, C.J., McClay, K.R., 1995. The geometry and evolution of a transpressional strike-slip system: the Carboneras Fault, SE Spain. Journal of the Geological Society, London 152, 339–351.

Kim, Y-S., Peacock, D.C.P., Sanderson, D.J., 2004. Fault damage zones. Journal of Structural Geology 26, 503–517.

Kleinschmidt, G., Tessensohn, F., 1987. Early Paleozoic westward directed subduction at the Pacific margin of Antarctica. In: McKenzie, G.D.M. (Ed.), Gondwana Six: Structure, Tectonics and Geophysics. AGU, Washington, DC, pp. 89–105.

Krantz, R.W., 1995. The transpressional strain model applied to strike-slip, oblique-convergent and oblique-divergent deformation. Journal of Structural Geology 17, 1125–1137.

Kyle, P.R., Cole, J.W., 1974. Strucutral controls of volcanism in the McMurdo volcanic Group, McMurdo Sound, Antarctica. Bulletin of Volcanology 38, 16–35.

Lawver, L.A., Gahagan, L.M., 1994. Constraints on timing of extension in the Ross Sea Region. Terra Antartica 1, 545–552.

Li, J.W., Zhou, M.F., Li, X.F., Fu, Z.R., Li, Z.J., 2001. The Hunan-Jangxi strike-slip fault system in southern China: southern termination of the Tan-Lu fault. Journal of Geodynamics 32, 333–354.

Little, T.A., 1996. Faulting-related displacement gradients and strain adjacent to the Awatere strike-slip fault in New Zealand. Journal of Structural Geology 18, 321–340.

Logan, J.M., Friedman, M., Higgs, N.G., Dengo, C., Shimamoto, T., 1979. Experimental studies of simulated gouge and their application to studies of natural fault zones. Open-File Report United States Geological Survey 79-1239, 305–343.

Lombardo, B., Cappelli, B., Carmignani, L., Gosso, G., Memmi, I., Montrasio, A., Palmeri, R., Pannuti, F., Pertusati, P.C., Ricci, C.A., Salvini, F., Talarico, F., 1989. The metamorphic rocks of the Wilson Terrane between David and Mariner glaciers, North Victoria Land, Antarctica. Memorie della Società Geologica Italiana 33, 99–130.

Ludman, A., 1998. Evolution of a transcurrent fault system in shallow crustal metasedimentary rocks: the Norumbega fault zone, eastern Maine. Journal of Structural Geology 20, 93–107.

Mandl, G., 2000. Faulting in Brittle Rocks. An Introduction to the Mechanics of Tectonic Faults. Springer, Berlin. 434pp.

Martel, S.J., 1990. Formation of compound strike-slip fault zones, Mount Abbot quadrangle, California. Journal of Structural Geology 12, 869–882.

Martel, S.J., 1997. Effects of cohesive zones on small faults and implications for secondary fracturing and fault trace geometry. Journal of Structural Geology 19, 835–847.

McGrath, A.G., Davison, I., 1995. Damage zone geometry around fault tips. Journal of Structural Geology 17, 1011–1024.

Moore, D.E., Byerlee, J., 1992. Relationships between sliding behavior and internal geometry of laboratory fault zones and some creeping and locked strike-slip faults of California. Tectonophysics 211, 305–316.

Moore, D.E., Summers, R., Byerlee, J.D., 1989. Sliding behavior and deformation textures of heated illite gouge. Journal of Structural Geology 11, 329–342.

Mukasa, S.B., Dalzier, I.W.D., 2000. Marie Byrd Land, West Antarctica: evolution of Gondwana's Pacific margin constrained by zircon U–Pb geochronology and feldspar common Pb isotopic composition. Geological Society of America Bulletin 112, 611–627.

Naylor, M.A., Mandl, G., Sijpesteijn, C.H.K., 1986. Fault geometries in basement-induced wrench faulting under different initial stress states. Journal of Structural Geology 8, 737–752.

Nur, A., Ron, H., Scotti, O., 1986. Fault mechanics and the kinematics of block rotations. Geology 14, 746–749.

Pachell, M.A., Evans, J.P., 2002. Growth, linkage, and termination processes of a 10-km-long strike-slip fault in jointed granite: the Gemini fault zone, Sierra Nevada, California. Journal of Structural Geology 24, 1903–1924.

Peacock, D.C.P., Anderson, M.W., Morris, A., Randall, D.E., 1998. Evidence for the importance of 'small' faults on block rotation. Tectonophysics 299, 1–13.

Petit, J.P., 1987. Criteria for the sense of movement on fault surfaces in brittle rocks. Journal of Structural Geology 9, 597–608.

Price, R.A., Carmichael, D.M., 1986. Geometric test for Late Cretaceous–Paleogene intracontinental transform faulting in the Canadian Cordillera. Geology 14, 468–471.

Richard, P., 1991. Experiments on faulting in a two-layer cover sequence overlying a reactivated basement fault with oblique slip. Journal of Structural Geology 13, 459–469.

Riedel, W., 1929. Zur mechanik geologischer brucherscheinungen. Zentralblatt für Mineralogie, Geologie und Paläontologie 1929B, 354–368.

Rispoli, R., 1981. Stress fields about strike-slip faults inferred from stylolites and tension gashes. Tectonophysics 75, T29–T36.

Rocchi, S., Tonarini, S., Armenti, P., Innocenti, F., Manetti, P., 1998. Geochemical and isotopic structure of the early Palaeozoic active margin of Gondwana in northern Victoria Land, Antarctica. Tectonophysics 284, 261–281.

Rocchi, S., Armenti, P., D'Orazio, M., Tonarini, S., Wijbrans, J., Di Vincenzo, G., 2002. Cenozoic magmatism in the western Ross Embayment: role of mantle plume vs. plate dynamics in the development of the West Antarctic Rift System. Journal of Geophysical Research 107, 2195–2217.

Roland, N.W., Läufer, A.L., Rossetti, F., 2004. Revision of the terrane model of North Victoria Land (Antarctica). Terra Antarctica 11, 55–65.

Rossetti, F., Storti, F., Salvini, F., 2000. Cenozoic noncoaxial transtension along the western shoulder of the Ross Sea, Antartica, and the emplacement of McMurdo dyke arrays. Terra Nova 12, 60–66.

Rossetti, F., Storti, F., Läufer, A., 2002. Brittle architecture of the Lanterman Fault and its impact on the final terrane assembly in North Victoria Land, Antarctica. Journal of the Geological Society of London 159, 159–173.

Rossetti, F., Lisker, F., Storti, F., Läufer, A., 2003. Tectonic and denudational history of the Rennick Graben (North Victoria Land): implications for the evolution of rifting between East and West Antarctica. Tectonics 22, 1016. doi:10.1029/2002TC001416.

Rossetti, F., Storti, F., Busetti, M., Lisker, F., Di Vincenzo, G., Läufer, A., Rocchi, S., Salvini, F., 2005. Eocene initiation of Ross Sea dextral faulting and implications for East Antarctic neotectonics. Journal of the Geological Society of London 162, 1–8.

Salvini, F., Storti, F., 1999. Cenozoic tectonic lineaments of the Terra Nova Bay region, Ross Embayment, Antarctica. Global and Planetary Change 23, 129–144.

Salvini, F., Brancolini, G., Busetti, M., Storti, F., Mazzarini, F., Coren, F., 1997. Cenozoic geodynamics of the Ross Sea Region, Antarctica: crustal extension, intraplate strike-slip faulting and tectonic inheritance. Journal of Geophysical Research 102, 24669–24696.

Salvini, F., Billi, A., Wise, D.U., 1999. Strike-slip fault-propagation cleavage in carbonate rocks: the Mattinata fault zone, Southern Apennines, Italy. Journal of Structural Geology 21, 1731–1749.

Schmoker, M., Bystricky, M., Kunze, K., Burlini, L., 2003. Granular flow and Riedel band formation in water-rich quartz aggregates experimentally deformed in torsion. Journal of Geophysical Research 108, 2242. doi:10.1029/2002JB001958.

Schreurs, G., 2003. Fault development and interaction in distributed strike-slip shear zones: an experimental approach. In: Storti, F., Holdsworth, R.E., Salvini, F. (Eds.), Intraplate Strike-slip Deformation Belts Geological Society, London, Sspecial Publication 210, pp. 35–52.

Skinner, D.N.B., Richer, J., 1968. The geology of the region between the Mawson and Priestley glaciers, north Victoria Land, Antarctica. New Zealand Journal of Geology and Geophysics 11, 1009–1040.

Storti, F., Rossetti, F., Salvini, F., 2001. Structural architecture and displacement accommodation mechanisms at the termination of the Priestley Fault, northern Victoria Land, Antarctica. Tectonophysics 341, 141–161.

Storti, F., Holdsworth, R.E., Salvini, F., 2003a. Intraplate strike-slip deformation belts. In: Storti, F., Holdsworth, R.E., Salvini, F. (Eds.), Intraplate Strike-slip Deformation Belts Geological Society, London, Special Publication 210, pp. 1–14.

Storti, F., Rossetti, F., Salvini, F., 2003b. Intracontinental accommodation of oceanic transform shear and the transtensional opening of Cenozoic deep basins at the northeastern edge of Antarctica. Geophysical Research Abstracts 5, 03082.

Sutherland, R., 1995. The Australia–Pacific boundary and Cenozoic plate motions in the SW Pacific—some constraints from Geosat data. Tectonics 14, 819–831.

Swan, A.R.H., Sandilands, M., 1995. Introduction to Geological Data Analysis. Blackwell, Oxford. 446pp.

Swanson, M.T., 1988. Pseudotachylyte-bearing strike-slip duplex structures in the Fort Foster Brittle Zone of southernmost Maine. Journal of Structural Geology 10, 813–828.

Sylvester, A.G., 1988. Strike-slip faults. Geological Society of America Bulletin 100, 1666–1703.

Tavani, S., Louis, L., Souque, C., Robion, P., Salvini, F., Frizon de Lamotte, D., 2004. Folding-related fracture pattern and physical properties of rocks in the Chaudrons ramp-related anticline (Corbières, France). In: Swennen, R., Roure, F., Granath, J.W. (Eds.), Deformation, Fluid Flow, and Reservoir Appraisal in Foreland Fold and Thrust Belts AAPG Hedberg Series 1, pp. 257–275.

Tchalenko, J.S., 1968. The evolution of kink-bands and the development of compression textures in sheared clays. Tectonophysics 6, 159–174.

Tchalenko, J.S., 1970. Similarities between shear zones of different magnitudes. Geological Society of America Bulletin 81, 1625–1640.

Umhoefer, P.J., 2000. Where are the missing faults in translated terranes? Tectonophysics 326, 23–35.

Vauchez, A., Pacheco-Neves, S., Caby, R., Corsini, M., Egydio-Silva, M., Arthaud, M., Amaro, V., 1995. The Borborema shear zone system. Journal of South American Earth Sciences 8, 247–266.

Weaver, S.D., Bradshaw, J.D., Laird, M.G., 1984. Geochemistry of Cambrian volcanics in northern Victoria Land, Antarctica. Earth and Planetary Science Letters 68, 128–140.

Wilson, T.J., 1995. Cenozoic transtension along the Transantarctic Mountains–West Antarctic rift boundary, Southern Victoria Land, Antarctica. Tectonics 14, 531–545.

Wise, D.U., Funiciello, R., Parotto, M., Salvini, F., 1985. Topographic lineament swarm: clues to their origin from domains analysis of Italy. Geological Society of America Bulletin 96, 952–967.

Woodcock, N.H., Schubert, C., 1994. Continental strike-slip tectonics. In: Hancock, P.L. (Ed.), Continental Tectonics. Pergamon Press, Oxford, pp. 251–263.